ISBN: 978-628-95207-8-1. ISSN: 2414-6390. Digital Object Identifier: 10.18687/LACCEI2024.1.1.908

Non-Invasive River Level Measurement Using Trainable Segmentation in Computer Vision

Federico José Machado Olivares, PhD[1], José Alberto Aguilar Marroquín, MSc[2]
[1,2]*Universidad Don Bosco, El Salvador, federico.machado.edu.sv, alberto.marroquin@udb.edu.sv*

***Abstract*– The importance of monitoring river levels in sectors of San Salvador has recently grown due to the increase in intense rains in recent years, particularly in the Tomayate River, located in the municipality of Apopa. Previously, the same authors have carried out research work that allows us to know the level of a high-risk river in the metropolitan area using computer vision, but the flood filling technique used, provides a very limited scope because it causes many errors when there is turbulence. In this work, the accuracy of level measurement has been significantly improved by applying a trainable segmentation technique, which provides a measurement error of less than 5% in about 68% of the processed images. This procedure will improve the development of early warnings of possible river flooding, thus reducing the risk of loss of material goods and human lives for those who live near the river.**

***Keywords*— computer vision, early warning, flood, river level, trainable segmentation.**

I. Introduction

In the metropolitan area of San Salvador, some rivers traverse densely populated areas and are prone to overflow during intense rains, whether short or long-lasting. This poses the risk of losses in both material goods and human lives [1]-[3].

Institutions such as National Civil Protection System of El Salvador (Sistema Nacional de Protección Civil de El Salvador) have recently joined a project aimed at creating a network of sensors to measure variables that help identify risks caused by nature. In the same line of action, the Planning Office of the Municipal Mayor of San Salvador (Oficina de Planificación del Área Metropolitana de San Salvador, OPAMSS) supervised a project for the installation of a sensor on the banks of the Tomayate River in Apopa, located 12 kilometers from the capital of El Salvador. [4]-[6]. Fig. 1a represents the geographical area of the Apopa municipality, while Fig. 1b provides an overview of the river, including a yellow arrow indicating the location where the sensor was installed in March 2023. This sensor is composed of a camera, a computer, and peripherals, including visual and audible indicators. With this system, the acquired images are analyzed and processed using the 'flood fill' algorithm, a module available in the OpenCV libraries. This project was developed by the same authors of this document and was presented at CONCAPAN XLI, Honduras, 2023, under the title *Python-based computer vision for non-intrusive river level measurement*.

Nevertheless, as the initial year of operation progressed, there was a rise in rainfall, leading to an expansion in the diversity of scenarios captured by the camera. This can be attributed to the impact of moisture on environmental surfaces, alterations in the shadow patterns of trees, and changes in other objects due to the precession movement of the Earth's equinoxes. Consequently, numerous measurements aligned visually with the water boundary, as illustrated in Fig. 2a, were deemed accurate. However, a considerable number of other measurements began to exhibit a noticeable error, as evidenced in Fig. 2b. This error was more recurrent when the water exhibited turbulence.

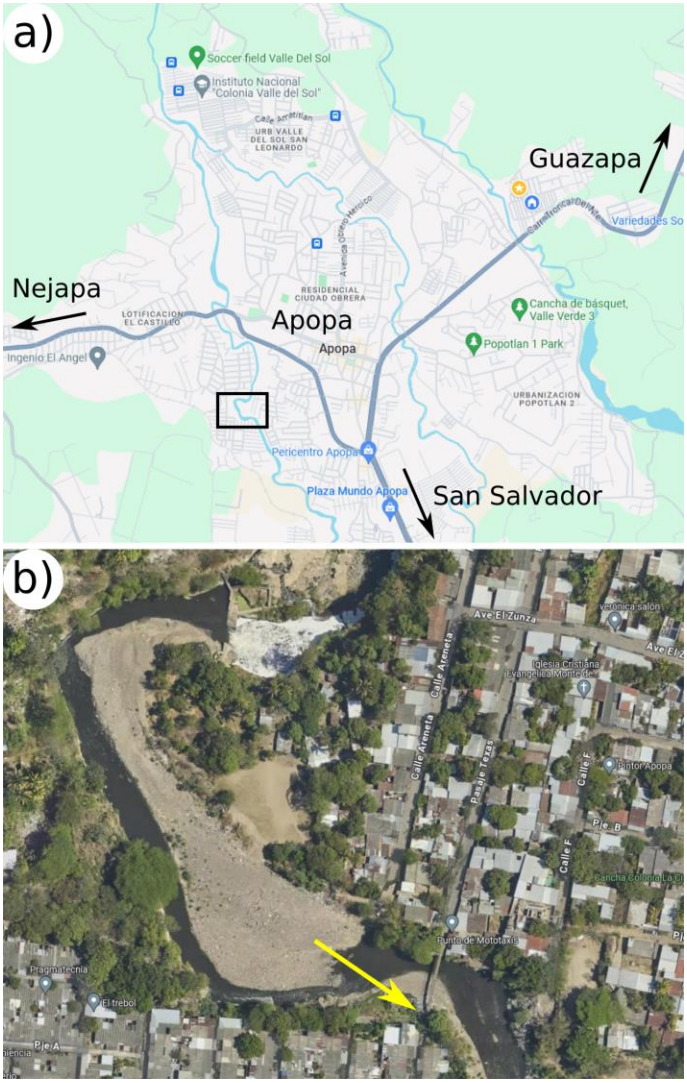

Fig. 1. Locations of the risk zone (a) Apopa, located 12 km north of San Salvador (b) View of the Tomayate River

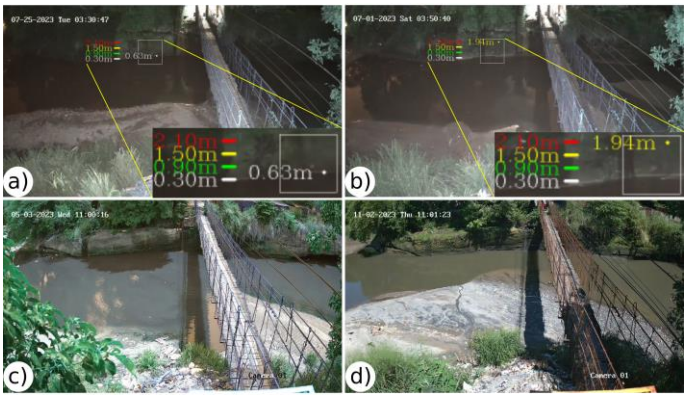

Fig. 2. Differences in measurements (a) Correct measurement, (b) Measurement with error and differences in shadow caused by the sun, (c) View month of May, (d) View month of November

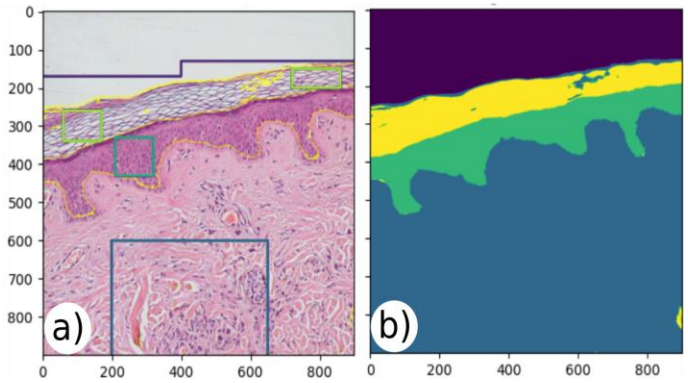

Fig. 3. Trainable segmentation technique applied to image, (a) Delimitation of areas that are used as labels, (b) Segmented areas.

One of the most influential factors in error production when using the flood-filling algorithm has been water turbulence and the precession movement of the equinoxes, as illustrated in Fig. 2c for May. In this month, shadows cause darkness and moisture on the slope, making it challenging for the algorithm to delineate a boundary for the water. In contrast, in the case of November, as shown in Fig. 2d, there is no longer any shadow, and the land at the water boundary remains drier.

Experience has shown that, under these conditions and with turbulent waters, the flood-filling algorithm frequently fails to determine the water level in the river, exhibiting sensitivity to variations in the lighting in the images, affecting the estimates [7]-[8]. Conventional tools also do not guarantee optimal performance, as they often involve measurement equipment installed directly in the river, and rapid rises in water levels with high turbulence can seriously impact their operation. Therefore, the idea of measuring the river level exclusively with information provided by a camera is maintained [9]-[11].

In this sense, it has been necessary to carry out a search for different techniques to measure the water level in rivers that represent a potential risk for people and material assets located near their area of influence. Among other criteria that must be evaluated, there are:

a) The sensor is not invasive. Because the Tomayate River rises very quickly in level and takes away any measuring instrument that is installed inside the water or on its shore.
b) Base your measurement solely based on images. Consequently, and taking advantage of the advances that technology has in image processing and artificial intelligence, we seek to use images as the only resource.
c) Determine the level measurement even with high turbulence. This implies, in terms of the images obtained, that the sensor determines the water level with various shades of color caused by water foam, garbage, flashes of light at night due to the brightness of different lighting sources and others.

Table I describes different investigations that meet the aforementioned criteria.

Of the sources consulted, none clearly addressed the problem of measuring the level when the river has high turbulence. This article presents the results of incorporating the trainable segmentation technique into the system algorithm to correct the limitations found in the first version of the project and the criteria not met in the sources consulted previously.

II. Methodology and Procedure

To overcome the difficulty caused by illumination, both during the day and at night, in the task of delineating the water level, the trainable segmentation technique shown in Fig. 3 has been applied. Pixel-based segmentation is determined using local functions as a basis, which include local intensity, edges, and textures at different scales. It is necessary to have a mask provided by the user to train a random forest classifier belonging to the scikit-learn module, available in Python. In the prediction process, the classifier will assign labels to pixels that have not been previously labeled [30]. This algorithm is explained in detail in [31] and has had applications in microscopy and radiology [32]-[33].

The recently methods use "trainable machine learning" and include small databases as an important part of the segmentation for labeling regions with a high degree of precision.

TABLE I
DIFFERENT TECHNIQUES USED TO MEASURE THE WATER LEVEL IN RIVERS.

Item	Invassive	Image	Addressed in
1	No	No	12, 13, 14, 15, 16, 17, 18
2	No	Yes	19, 20, 21, 22, 23, 24
3	Yes	No	25, 26
4	Yes	Yes	27, 28, 29

The mathematical procedure is based on an algorithm known as WEKA (Waikato Environment for Knowledge Analysis) through the construction of its decision trees. These decision trees allow pixels to be classified and, during the process used by Trainable Weka Segmentation (TWS), the main features of the image are extracted through the native processes of the Fiji algorithm; subsequently, a set of pixel samples are defined as vectors corresponding to the same function and the WEKA learning scheme is trained with these samples to finally apply an inference process to the remaining pixels of the image. More details on [34]-[36].

When using the trainable segmentation algorithm, the user must label zones in the input image with consecutive numbers starting from 1 (Fig. 3a). Upon applying segmentation, the algorithm produces a new image composed of masks, each identified with a color, assigning the labels of the delimited zones in the input image (Fig. 3b) to those areas not labeled in the original image. It is essential to highlight that:

- It is only necessary to delineate some regions in the input image, which should be representative of the sections that will be labeled in the output image.
- In the specific case of the Tomayate River, it has been necessary to outline 2 regions in the input image: the first where there is always water, and a second that shows vegetation and land. There is a region intentionally left without a label, where it is expected that the trainable segmentation algorithm will determine the presence or absence of water, aiding in determining the water level.

The reason why this algorithm was chosen specifically, instead of opting to obtain a history of images to train a neural network that encompasses all possible scenarios, is because it allows the inclusion of:

- A images history containing water in the river.
- A portion of the current image, where it is previously known that there is water, and whose color, texture, and edge characteristics, among others, will contribute to identifying water in unlabeled areas.

Due to the different conditions that affect the obtained images, such as lighting variations throughout the year caused by the sun's shadow, clouds or sunlight, day or night, rain or no rain, among others, the system must be trained to establish the difference between water and land-vegetation. Therefore, a historical set of photos taken between February and August 2023 has been utilized, selecting scenarios both during the day and at night, with and without storms. This has allowed training the algorithm with a modest diversity of situations.

Fig. 4 illustrates the procedure carried out to identify the areas with water in a section of the Tomayate River. Initially, an image of the river is obtained with a resolution of 1920x720 pixels (Fig. 4a), and a portion of it represents the region of interest with a resolution of 388x310 pixels (Fig. 4c). The historical images captured by the camera have allowed the extraction of portions with different scenarios, forming the image manually built in (Fig. 4b). This image has 12 rows, where the upper 6 identify the land-vegetation content at a level where it is anticipated that the river water will never reach, and the lower 6, where there is always water.

To establish a better correlation between the water level and the risk it represents for the communities that live very close to the river, several visits have been made to the site and conversations have been held with people who have lived there for several years. They have correlated the water level with the length of time a rain has lasted and its intensity. With this information and the images that have been taken with the camera in the first rainy months of 2023, the yellow, green and red alert levels that have been marked in each of the processed images have been determined. In this way, images (Fig. 4b) and (Fig. 4c) are merged to create a unified input image denoted as (4b-4c), equivalent to Fig. 3a as the algorithm input. This input undergoes changes in each iteration owing to real-time updates from the camera. Zone labels in this context are assigned through an additional image, denoted as (Fig. 4d), with color codes corresponding as follows:

- Yellow: water.
- Blue: land-vegetation.
- Black: unlabeled zone, anticipated to be classified by the algorithm.

In Fig. 4e, it is better appreciated how the subarea of Fig. 4d overlaps in the region of interest of the image captured by the camera. When applying the trainable segmentation algorithm with the image 4b-4c, only the subarea shown in Fig. 4d is selected, thus generating the resulting image Fig. 4f where the white color indicates the presence of water. In Fig. 4g, the comparison of the area of interest, marked by a rectangle, is observed, and, on one side, the region containing water is delimited in white. The general algorithm used for the sensor's operation is shown in Fig. 5, where:

a) *Load imageRef and maskRef into variables*: Load the reference image "imageRef" depicted in Fig. 4b and the image containing labeled areas, shown in Fig. 4d, and referred to as "MaskRef," into system memory.
b) *Get img-i from camera*: Capture the image from the camera.
c) *Get ROI from img-i*: Extract a specific region of interest from the camera image, delineated by a predefined region established within the algorithm.
d) *Build img_i_ref from img-i and imageRef*: Create an image, denoted as img_i_ref, by combining the image obtained in step (a) with the region of interest obtained in step (c). This resulting image will be represented by 4b-4c.
e) *Get mask of segmented image from imageRef and MaskRef*: the system runs the trainable segmentation algorithm, which takes the figure 4b-4c and the

labeled areas of Fig. 4d, to generate estimates like shown in Fig. 4f.

f) *Calculate px_height and height*: Calculates, based on a relationship between pixels and heights of reference points in the river, the coordinates of a pixel representing the water boundary "px_height" and subsequently calculates the water height "height."

g) The algorithm for this block is explained in the following flowchart.

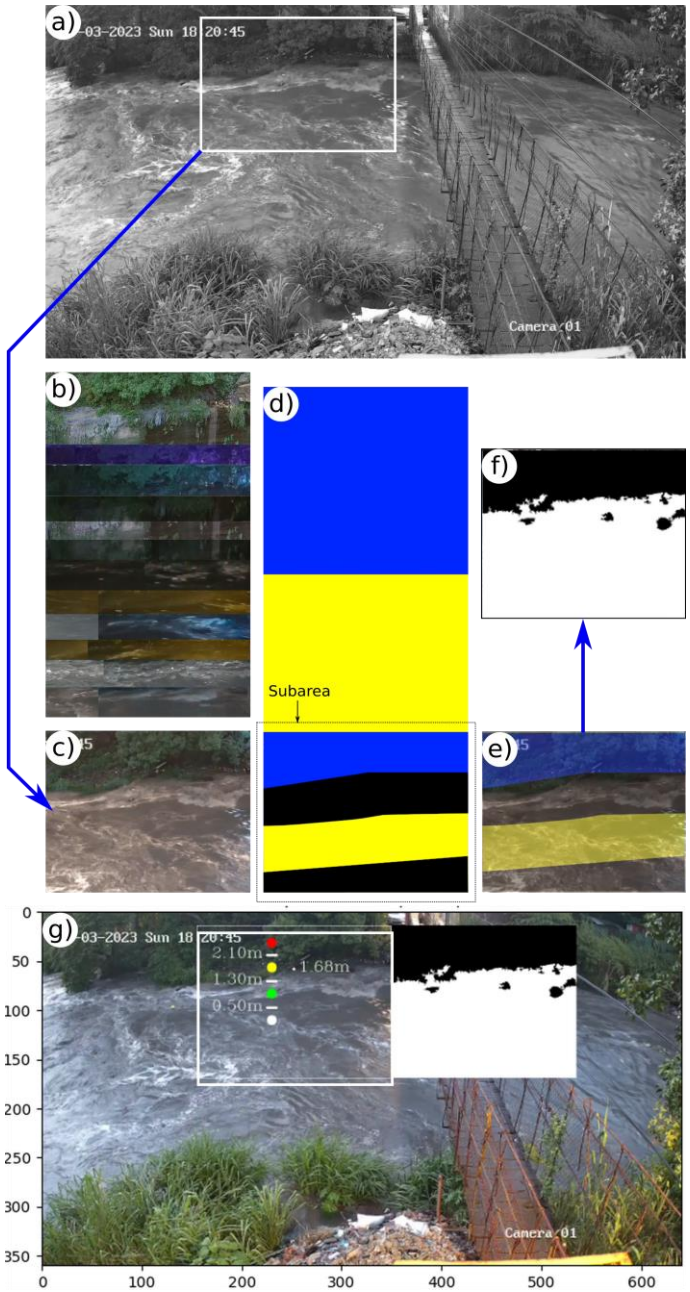

Fig. 4. Procedure used in the trainable segmentation algorithm to segment areas with water

h) *Send results to MQTT broker, register image and text logging*: The sensor sends the previously calculated river water level to an MQTT broker, using this protocol because it is expected to be part of a network of similar sensors for monitoring other rivers under similar conditions. Additionally, an image of the river without processing is stored, another processed image, and finally, a line with the level information is added to a CSV file, thus enriching the historical record of river images.

i) *Get new image*: The camera is taking pictures of the river 24/7 and will only stop when the technician orders the program's termination. Every 30 seconds, an image is processed to trigger an alarm based on the water level, and, based on the triggered alarm if any, the cycle of this flowchart repeats.

It is considered that the segmentation produced in a portion of the river image has a white color where there is water and black where there is none, as illustrated in Fig. 4f.

To determine the water level using a monochrome image, the following phases described in the algorithm shown in Fig. 6 are applied:

a) *Load mask of segmented image into a variable*: The monochromatic image obtained from segmentation is loaded into a variable. This image has dimensions of the area of interest, 388x310 pixels.

b) *Calculate average value on row-i*: Starting with the value of i = 309, the position of the pixel at the bottom of the region of interest, calculate the average value of the 310 pixels in the corresponding row. These pixels have binary values of 0 or 255.

c) *Average is less than threshold?*: The average of the pixels in an i-th row is represented as a percentage, so the variable "average" is a float with values between 0 and 1; "threshold" has a value of 0.5, chosen to visually ensure 50% with water. If the average is less than the threshold, it continues to step (d); otherwise, it proceeds to step (e).

d) *Calculate height based on the value of i*: The value of i corresponds to the pixel position that serves as a representative indicator of the presence of water. To determine the water height in the river, an interpolation of px and height values described in Table 1 is carried out. At this point, the calculation of the water level in the river for a camera capture concludes.

e) *Decrement i*: Decrease the value of i.

f) *Is i equal to 0?*: If i is equal to zero, it signifies that the highest position in the image has been reached. Consequently, proceed to step (g) establishing that the maximum height has been reached.

g) *Height = maximum*: Set the maximum height to 2.5m. This value should alert the reader to a potential error in this measurement, concluding this calculation.

This condition rarely occurs and is attributed to very intense rainfall or foggy conditions on the scene. Additionally, it has been verified that a subsequent image taken a few minutes later does not necessarily eliminate the error condition in the measurement because the measurement fundamentally depends on the scene. It is advisable to wait for the next cycle of measurements, which, under high-level conditions, will occur in 5 minutes.

The relationship between the pixels used to determine the water height and the water level in the river is determined by Table II.

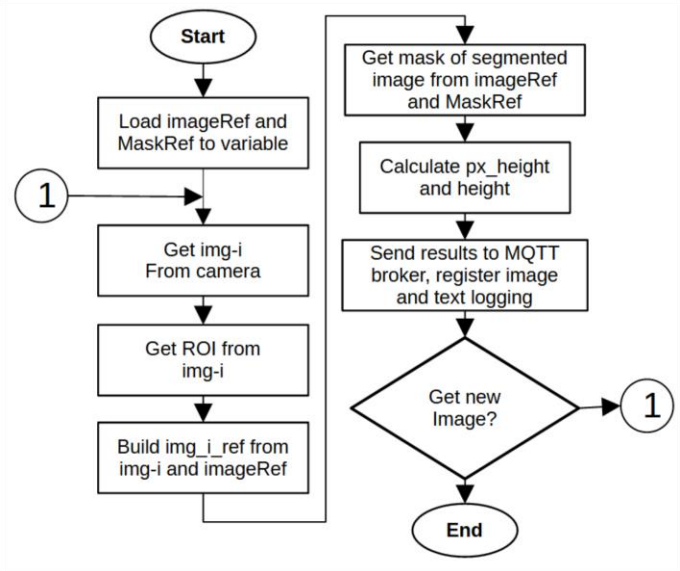

Fig. 5. General algorithm for system operation

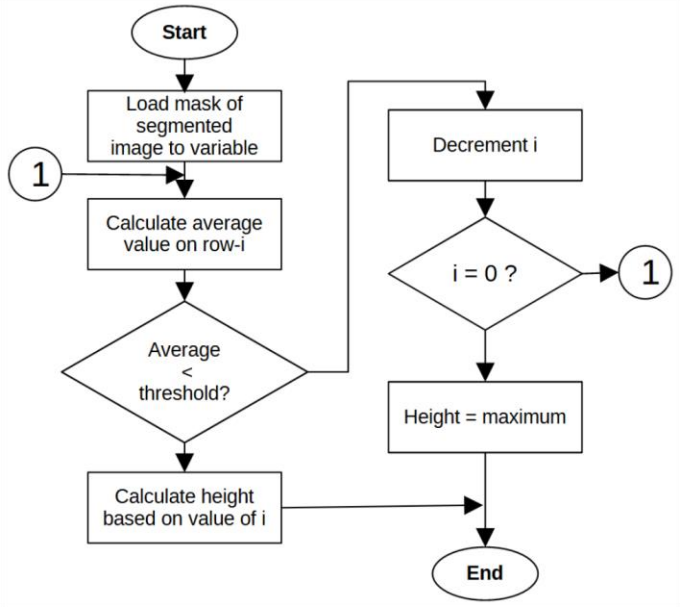

Fig. 6. Algorithm to determine water level from segmentation

TABLE II:
THRESHOLD BETWEEN ALERTS AND RELATIONSHIP WITH PIXELS IN IMAGE AND HEIGHT IN RIVER.

Px	Height [m]	Threshold between alerts
147	0.8	White – Green
107	1.4	Green – Yellow
67	2.0	Yellow – Red

TABLE III:
CALCULATION OF THE ERROR DETERMINED BY THE PIXEL COORDINATES VISUAL MARKING THE RIVER LEVEL (Y) AND MEASUREMENT CALCULATED BY THE ALGORITHM (Y1).

Item	Datetime / Identifier	x	y	y1	Error %
1	2023Apr16 201552	563	178	191	7.3%
2	2023Apr16 201709	563	178	188	5.6%
3	2023Apr16 201935	563	181	191	5.5%
4	2023Apr16 202523	563	180	189	5.0%

TABLE IV:
PERCENTAGES ASSOCIATED WITH ERROR CATEGORIZATION AND QUANTITY IN RIVER LEVEL MEASUREMENTS.

Categories	Quantity	Percentage
< 3%	2964	16.91%
<= 3% and < 5%	9110	51.98%
<= 5% and <8%	3835	21.88%
<= 8% and <10%	289	1.65%
> 10%	1327	7.57%
Totals	17525	100.0%

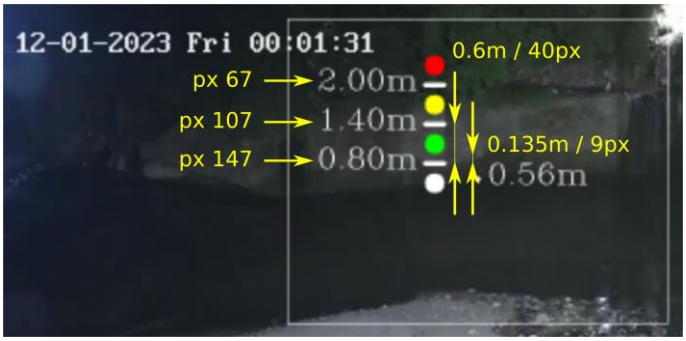

Fig. 7. Relationship between pixels in the captured image and heights in the river water level

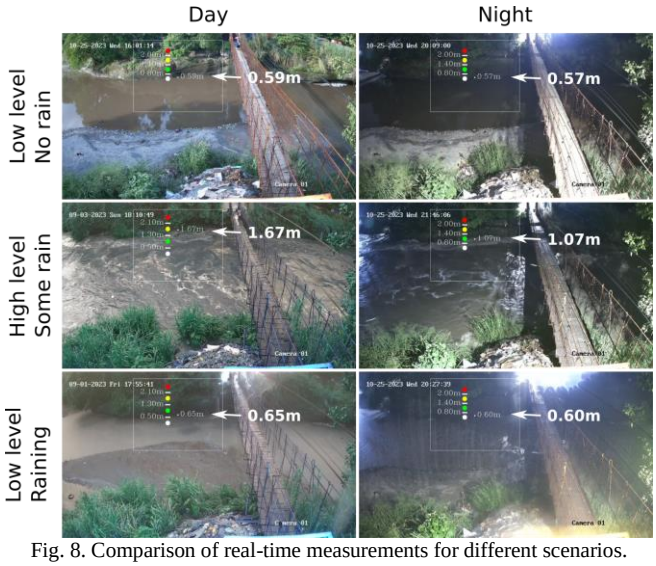

Fig. 8. Comparison of real-time measurements for different scenarios.

When making a comparison with level measurements carried out under different circumstances, which include day and night, low level with very little turbulence and high level with a lot of turbulence, as well as rainy or non-rainy conditions, the results are found to be satisfactory according to are shown in figure 8.

III. Results

The results between manually determined river height values through an image record and those calculated through the trainable segmentation algorithm total 17,525 data points. Some random data is shown in Table III, where the visual measurement made by a person with an image in front of the computer is considered the reference for error calculation. The measurements span from the first half of February to the first half of November 2023, covering the rainy season in El Salvador during the first year of the project.

Table III shows the percentages associated with the categorization of error. As seen in the results, the behavior follows a normal curve, and for the categories that include "<3%" and "<= 3% and < 5%", a total of 12,074 measurements are summed up, representing 68.9% of the total.

Meaning of the 5% error in terms of pixels and river level.

According to the level measurement taken on April 16, 2023, at 20:25:23, for the last item in Table II, the pixel coordinates used to manually determine the water level are 180, while those determined by the algorithm are 189, resulting in a Δpx difference of 9. This indicates that, for 68.9% of measurements, the maximum error in determining the river level has been 9 pixels.

Referring to Fig. 7 and corresponding to Table I, the visual difference between the water level and the thresholds set for alerts can be observed. The difference between thresholds is 40 pixels, equivalent to 0.6m. It is noted that, for the 5% error, the distance equivalent to 9 pixels in the image is significantly smaller than the difference between two alert thresholds. Based on the experience gained during field visits to the location, it can be stated that this visual difference is sufficient to provide reliability in the system measurement with the trainable segmentation algorithm.

IV. Conclusions

- The trainable segmentation algorithm has succeeded in overcoming errors in determining the water level, as shown by the previous flood-filling algorithm. This is because it has now allowed the incorporation of portions of images from a history illustrating different scenarios of rain, darkness, and shadows, as well as parts of the current image. This enriches the information used to train the neural network of the segmentation algorithm.
- By totaling 68.9% of measurements with an error of less than 5% of the calculated value, it is considered that there is a high agreement with manually obtained visual values. This implies that the system has an acceptable margin of accuracy.
- When it is visually determined that a large number of measurements are less than 5%, observing an image of the river, it can be validated that the measurements obtained by the algorithm allow for a good level of clarity and reliability in defining the alert level. This informs people living near the river to take action to reduce losses in property and lives when the level rises significantly.

Acknowledgment

This project for the installation of a sensor for early warning in the Tomayate River has been made possible by the funding from Andalusian Agency for International Cooperation (Agencia Andaluza de Cooperación Internacional), under the contract administration of the OPAMSS, and the technical design by the authors of this publication.

References

[1] Perfil de riesgo de desastre por inundaciones para El Salvador: Informe nacional, BID. https://publications.iadb.org/es/publicacion/15578/perfil-de-riesgo-de-desastre-por-inundaciones-para-el-salvador-informe-nacional

[2] Gestión de Riesgos urbanos Inundaciones Urbanas en El Salvador, SNET. https://www.snet.gob.sv/Publicaciones/InundacionesUrbanas.PDF

[3] Plan de recuperación de ríos urbanos, MARN. http://rcc.marn.gob.sv/handle/123456789/8

[4] Inundaciones: un fenómeno recurrente en la ciudad de San Salvador, FUNDASAL. http://repo.fundasal.org.sv/176/

[5] Plan Nacional de Adaptación al Cambio Climático, MARN. http://rcc.marn.gob.sv/handle/123456789/371

[6] Perspectivas del Medio Ambiente Urbano, CCAD. https://wedocs.unep.org/handle/20.500.11822/9389

[7] G. Zhang, Z. Luo, Y. Chen, Y. Zheng and W. Lin, "Illumination Unification for Person Re-Identification," *Transactions on Circuits and Systems for Video Technology*, vol. 32, no. 10, pp. 6766-6777, Oct. 2022

[8] K. Song, L. Huang, A. Gong and Y. Yan, "Multiple Graph Affinity Interactive Network and a Variable Illumination Dataset for RGBT Image Salient Object Detection," *Transactions on Circuits and Systems for Video Technology*, vol. 33, no. 7, pp. 3104-3118, July 2023. doi: 10.1109/TCSVT.2022.3169422.

[9] G. Dou, R. Chen, C. Han, Z. Liu, and J. Liu, "Research on Water-Level Recognition Method Based on Image Processing and Convolutional Neural Networks," *Water*, vol. 14, no. 12. MDPI AG, p. 1890, Juny 2022. doi: 10.3390/w14121890.

[10] F. Xia, H. Zhang, G. Zhang, D. Peng, and H. Li, "Image Processing in the Monitor of Boiler Drum Water Level on Power Plant," *Energy Procedia*, vol. 17. Elsevier BV, pp. 266–272, 2012. doi: 10.1016/j.egypro.2012.02.093.

[11] G. Chen et al., "Method on water level ruler reading recognition based on image processing," *Signal, Image and Video Processing*, vol. 15, no. 1. Springer Science and Business Media LLC, pp. 33–41, Jun. 16, 2020. doi: 10.1007/s11760-020-01719-y.

[12] R. Sulistyowati, H. A. Sujono, and A. K. Musthofa, "Design and field test equipment of river water level detection based on ultrasonic sensor and SMS gateway as flood early warning," AIP Conference Proceedings. Author(s), 2017. doi: 10.1063/1.4985517.

[13] A. Kalyanapu, C. Owusu, T. Wright, and T. Datta, "Low-Cost Real-Time Water Level Monitoring Network for Falling Water River Watershed: A Case Study," Geosciences, vol. 13, no. 3. MDPI AG, p. 65, Feb. 26, 2023. doi: 10.3390/geosciences13030065.

[14] J. N. Kabi, C. wa Maina, E. T. Mharakurwa, and S. W. Mathenge, "Low cost, LoRa based river water level data acquisition system," HardwareX, vol. 14. Elsevier BV, p. e00414, Jun. 2023. doi: 10.1016/j.ohx.2023.e00414.

[15] A. Prafanto and E. Budiman, "A Water Level Detection: IoT Platform Based on Wireless Sensor Network," 2018 2nd East Indonesia Conference on Computer and Information Technology (EIConCIT). IEEE, Nov. 2018. doi: 10.1109/eiconcit.2018.8878559.

[16] I. H. Abd Halim, A. I. Mahamad, and M. F. Mohd Fuzi, "Automated Alert System for River Water Level and Water Quality Assessment using Telegram Bot API," Journal of Computing Research and Innovation, vol. 6, no. 3. UiTM Press, Universiti Teknologi MARA, pp. 65–74, Sep. 13, 2021. doi: 10.24191/jcrinn.v6i3.234.

[17] N. M. Fathur Rahman, S. Manjang, and Z. Zainuddin, "Water level monitoring using ultrasonic-pipe in open channel," 2017 15th International Conference on Quality in Research (QiR) : International Symposium on Electrical and Computer Engineering. IEEE, Jul. 2017. doi: 10.1109/qir.2017.8168493.

[18] A. Galli, C. Peruzzi, F. Gangi, and D. Masseroni, "ArduHydro: a low-cost device for water level measurement and monitoring," Journal of Agricultural Engineering. PAGEPress Publications, Jan. 23, 2024. doi: 10.4081/jae.2024.1554.

[19] J. A. Azevedo and J. A. Brás, "Measurement of Water Level in Urban Streams under Bad Weather Conditions," Sensors, vol. 21, no. 21. MDPI AG, p. 7157, Oct. 28, 2021. doi: 10.3390/s21217157.

[20] W.-C. Liu and W.-C. Huang, "Evaluation of deep learning computer vision for water level measurements in rivers," Heliyon, vol. 10, no. 4. Elsevier BV, p. e25989, Feb. 2024. doi: 10.1016/j.heliyon.2024.e25989.

[21] R. Vandaele, S. L. Dance, and V. Ojha, "Deep learning for automated river-level monitoring through river-camera images: an approach based on water segmentation and transfer learning," Hydrology and Earth System Sciences, vol. 25, no. 8. Copernicus GmbH, pp. 4435–4453, Aug. 16, 2021. doi: 10.5194/hess-25-4435-2021.

[22] R. Vandaele, S. L. Dance, and V. Ojha, "Calibrated river-level estimation from river cameras using convolutional neural networks," Environmental Data Science, vol. 2. Cambridge University Press (CUP), 2023. doi: 10.1017/eds.2023.6.

[23] M. Cahyadi, A. Bawasir, Susilo, and S. Arief, "Analysis of Water Level Monitoring using GNSS Interferometric Reflectometry in River Waters," IOP Conference Series: Earth and Environmental Science, vol. 1276, no. 1. IOP Publishing, p. 012020, Dec. 01, 2023. doi: 10.1088/1755-1315/1276/1/012020.

[24] Y. Sermet and I. Demir, "Camera-based intelligent stream stage sensing for decentralized environmental monitoring," Journal of Hydroinformatics, vol. 25, no. 2. IWA Publishing, pp. 163–173, Feb. 15, 2023. doi: 10.2166/hydro.2023.032.

[25] E. K. Wati, H. H. Santoso, and A. Laksono, "IOT-BASED WATER LEVEL MONITORING SYSTEM OF SITU RAWA BESAR," MSJ : Majority Science Journal, vol. 2, no. 1. PT. Hafasy Dwi Nawasena, pp. 219–231, Feb. 27, 2024. doi: 10.61942/msj.v2i1.89.

[26] M. T. Tabada Jr., M. E. Loretero, and F. F. Lasta Jr., "Investigation on the performance of a multi-wire water level detection system using contact sensing for river water monitoring," SN Applied Sciences, vol. 2, no. 1. Springer Science and Business Media LLC, Dec. 13, 2019. doi: 10.1007/s42452-019-1887-0.

[27] S. Noto, F. Tauro, A. Petroselli, C. Apollonio, G. Botter, and S. Grimaldi, "Low-cost stage-camera system for continuous water-level monitoring in ephemeral streams," Hydrological Sciences Journal, vol. 67, no. 9. Informa UK Limited, pp. 1439–1448, Jun. 16, 2022. doi: 10.1080/02626667.2022.2079415.

[28] F. Birgand, K. Chapman, A. Hazra, T. Gilmore, R. Etheridge, and A.-M. Staicu, "Field performance of the GaugeCam image-based water level measurement system," PLOS Water, vol. 1, no. 7. Public Library of Science (PLoS), p. e0000032, Jul. 21, 2022. doi: 10.1371/journal.pwat.0000032.

[29] L. K. S. Tolentino et al., "Real Time Flood Detection, Alarm and Monitoring System Using Image Processing and Multiple Linear Regression," SSRN Electronic Journal. Elsevier BV, 2023. doi: 10.2139/ssrn.4319789.

[30] Trainable segmentation using local features and random forests, scikit-image team. https://scikit-image.org/docs/stable/auto_examples/segmentation/plot_trainable_segmentation.html

[31] I. Arganda-Carreras et al., "Trainable Weka Segmentation: a machine learning tool for microscopy pixel classification," *Bioinformatics*, vol. 33, no. 15. Oxford University Press (OUP), pp. 2424–2426, Mar. 30, 2017. doi: 10.1093/bioinformatics/btx180.

[32] C. G. Bell, K. P. Treder, J. S. Kim, M. E. Schuster, A. I. Kirkland, and T. J. A. Slater, "Trainable segmentation for transmission electron microscope images of inorganic nanoparticles," *Journal of Microscopy*, vol. 288, no. 3. Wiley, pp. 169–184, May 11, 2022. doi: 10.1111/jmi.13110.

[33] Mr. N. Kanuri, Dr. A. Abdelkarim, and Dr. S. A. Rathore, "Trainable Weka segmentation tool machine learning-enabled segmentation on features of orthopantomograms," *Oral Surgery, Oral Medicine, Oral Pathology and Oral Radiology*, vol. 134, no. 3. Elsevier BV, p. e77, Sep. 2022. doi: 10.1016/j.oooo.2022.04.025.

[34] Z. Duran, İ. Akargöl, and T. Doğan, "Data Mining, Weka Decision Trees," Orclever Proceedings of Research and Development, vol. 3, no. 1. Orclever Science and Research Group, pp. 401–416, Dec. 31, 2023. doi: 10.56038/oprd.v3i1.376.

[35] W. Ibrahim, S. Abdullaev, H. Alkattan, O. A. Adelaja, and A. A. Subhi, "Development of a Model Using Data Mining Technique to Test, Predict and Obtain Knowledge from the Academics Results of Information Technology Students," Data, vol. 7, no. 5. MDPI AG, p. 67, May 23, 2022. doi: 10.3390/data7050067.

[36] S. M. F. D. Syed Mustapha, "Predictive Analysis of Students' Learning Performance Using Data Mining Techniques: A Comparative Study of Feature Selection Methods," Applied System Innovation, vol. 6, no. 5. MDPI AG, p. 86, Sep. 29, 2023. doi: 10.3390/asi6050086.